

THESIS

DOWNSCALING SOIL MOISTURE OVER REGIONS THAT INCLUDE MULTIPLE
COARSE-RESOLUTION GRID CELLS

Submitted by

Dylan C. Hoehn

Department of Civil and Environmental Engineering

In partial fulfillment of the requirements

For the Degree of Master of Science

Colorado State University

Fort Collins, Colorado

Fall 2016

Master's Committee:

Advisor: Jeffrey D. Niemann

Timothy R. Green
Stephanie K. Kampf

Copyright by Dylan Chase Hoehn 2016

All Rights Reserved

ABSTRACT

DOWNSCALING SOIL MOISTURE OVER REGIONS THAT INCLUDE MULTIPLE COARSE-RESOLUTION GRID CELLS

Many applications require soil moisture estimates over large spatial extents (30-300 km) and at fine-resolutions (10-30 m). Remote-sensing methods can provide soil moisture estimates over very large spatial extents (continental to global) at coarse resolutions (10-40 km), but their output must be downscaled to reach fine resolutions. When large spatial extents are considered, the downscaling procedure must consider multiple coarse-resolution grid cells, yet little attention has been given to the treatment of multiple grid cells. The objective of this paper is to compare the performance of different methods for addressing multiple coarse grid cells. To accomplish this goal, the Equilibrium Moisture from Topography, Vegetation, and Soil (EMT+VS) downscaling model is generalized to accept multiple coarse grid cells, and two methods for their treatment are implemented and compared. The first method (fixed window) is a direct extension of the original EMT+VS model and downscales each coarse grid cell independently. The second method (shifting window) replaces the coarse grid cell values with values that are calculated from windows that are centered on each fine grid cell. The window values are weighted averages of the coarse grid values within the window extent, and three weighting methods are considered (box, disk, and Gaussian). The methods are applied to three small catchments with detailed soil moisture observations and one large region. The fixed window typically provides more accurate estimates of soil moisture than the shifting window, but it produces abrupt

changes in soil moisture at the coarse grid boundaries, which may be problematic for some applications. The three weighting methods produce similar results.

ACKNOWLEDGMENTS

I gratefully acknowledge financial support from the Army Research Lab (ARL) Small Business Innovative Research (SBIR) program. I also thank Dr. Jeffrey Niemann, Stephanie Kampf, Tim Green, Andy Jones, Pete Grazaitis, Garret Cowley, and Mark Cammarere for their helpful suggestions and collaboration on this project.

TABLE OF CONTENTS

ABSTRACT.....	ii
ACKNOWLEDGMENTS.....	iv
1. INTRODUCTION.....	1
2. METHODOLOGY.....	6
2.1 EMT+VS MODEL OVERVIEW.....	6
2.2 GENERALIZATION TO MULTIPLE COARSE GRID CELLS.....	10
3. APPLICATION TO TEST SITES.....	13
3.1 TEST SITE PROPERTIES.....	13
3.2 MODEL APPLICATION.....	15
4. RESULTS AND DISCUSSION.....	17
5. CONCLUSION.....	25
6. FIGURES.....	28
7. REFERENCES.....	39
8. APPENDICES.....	45
8.1 APPENDIX A.....	45
8.2 APPENDIX B.....	46
8.3 APPENDIX C.....	47

1. INTRODUCTION

Numerous applications can benefit from knowledge of volumetric water content (soil moisture) at fine resolutions (10-30 m) over large spatial extents (30-300 km). For example, land-atmosphere models [Delworth and Manabe, 1989, Entekhabi et al., 1996, Ferranti and Viterbo, 2006], precipitation forecasting models [Koster and Suarez, 2003, Seuffert et al., 2002], regional and global climate models [Dirmeyer, 1999, Mahfouf et al., 1987, Seuffert et al., 2002], and hydrologic models at all scales [Houser et al., 1998, Lakshmi, 1998, Wood, 1997] would benefit from reliable soil moisture information. Similarly, soil moisture is important for flood forecasting [Beck et al., 2009, Dunne and Black, 1970], drought monitoring and wildfire prediction [Bartsch et al., 2009, Bolten et al., 2010], crop growth and forest regrowth after wildfires [de Wit and van Diepen, 2007, Kasischke et al., 2007], and malaria outbreak modeling [Montosi et al., 2012]. Soil moisture is an important variable in soil mechanical stability [Horn and Fleige, 2003], which is relevant in trafficability [Flores et al., 2014] and vehicle impact assessment and land rehabilitation [Shoop et al., 2005, Vero et al., 2014].

Satellite remote sensing can provide soil moisture estimates with the spatial extents necessary for such applications, but the spatial resolutions of these estimates are much too coarse. Several passive radiometers have been used to obtain global soil moisture at coarse resolutions. For example, the Advanced Microwave Scanning Radiometer (AMSR-E) uses dual polarized size frequencies in the range of 6.9-89 GHz to estimate soil moisture at resolutions of 5-60 km, where the coarser resolutions have smaller errors than the finer resolutions [Njoku et al., 2003]. Li et al. [2010] describes a physically-based land algorithm that simultaneously acquires global soil moisture, vegetation water content, and land surface temperature using

WindSat dual polarized data at 10, 18.7, and 37 GHz, resulting in 10-40 km resolution soil moisture estimates. The Soil Moisture Ocean Salinity Mission (SMOS) uses an L-band (1.4 GHz) synthetic aperture radiometer to estimate soil moisture and ocean salinity at a 40 km resolution [Kerr *et al.*, 2012, Kerr *et al.*, 2010]. Active microwave sensing has also been used to estimate soil moisture. In particular, the Advanced Scatterometer (ASCAT) produces backscatter measurements from transmitted linear frequency-modulated pulses (C-band) to estimate global soil moisture at a 25 km resolution [Bartalis *et al.*, 2007]. The Soil Moisture Active and Passive (SMAP) mission combines active and passive microwave sensing to obtain 9 km resolution global soil moisture, but currently only the passive radiometer is operational [Das *et al.*, 2011, Entekhabi *et al.*, 2010].

One general approach for downscaling soil moisture to appropriate resolutions is to use optical/thermal data. Such methods typically downscale to about a 1 km resolution because the most frequently collected optical/thermal data are available at this resolution. For example, Chauhan *et al.* [2003] downscaled soil moisture from 25 km to 1 km using an approach based on the Triangle Method. Merlin *et al.* [2005] downscaled 40 km SMOS data to a 1 km resolution using visible, near-infrared, and thermal infrared remote sensing data. Merlin *et al.* [2006] added the use of a land surface model and tested this approach. Disaggregation Based on Physical and Theoretical Scale Change (DisPATCH) was also used to downscale SMOS data to 3 km and 100 m resolutions using Moderate Resolution Imaging Spectroradiometer (MODIS), Advanced Spaceborne thermal Emission and Reflection radiometer (ASTER), and Landsat 7 data [Merlin *et al.*, 2013]. Fang and Lakshmi [2014] disaggregated SMOS and AMSR-E data to a 1 km resolution and compared the results to in situ observations. Using similar data in an empirical

algorithm, *Song et al.* [2014] downscaled 25 km AMSR-E data to 1 km using optical/thermal data, and it was more effective for soil moisture values less than $0.3 \text{ m}^3/\text{m}^3$.

Another group of downscaling methods focus on reproducing the statistical properties of fine scale soil moisture rather than providing accurate estimates at every location. For example, *Crow et al.* [2000] used a statistical approach to downscale spaceborne imaging radar (SIR-C) L-band data. They studied how patterns with 800-6400 m grid cells relate to finer (100-800 m) patterns. *Kim and Barros* [2002] used a modified fractal interpolation method based on contraction mapping to downscale soil moisture from 10 km to 825 m. *Mascaro et al.* [2011] applied a multifractal downscaling model to obtain soil moisture at the aircraft footprint scale of 800 m from a satellite footprint scale of 25.6 km.

Other statistical methods have been used to estimate soil moisture at fine resolutions. *Perry and Niemann* [2007] applied an Empirical Orthogonal Function (EOF) approach to the Tarrawarra catchment (downscaling from a catchment-wide average to a 20 m by 10 m resolution). However, this method requires local soil moisture measurements to derive the EOFs. In a similar manner, *Kaheil et al.* [2008] downscaled soil moisture based on local measurements. The Southern Great Plains (SGP 97) dataset (from airborne imagery) was downscaled from a coarse resolution of 800 m to a fine resolution of 50 m.

Other downscaling methods use topographic data, which is known to affect soil moisture variations at particularly fine resolutions [*Famiglietti et al.*, 1998, *Gomez-Plaza et al.*, 2001, *Western et al.*, 1999]. *Wilson et al.* [2005] downscaled soil moisture in five catchments to 10-40 m resolutions using empirical relationships with topographic attributes. *Busch et al.* [2012] extended the EOF method of *Perry and Niemann* [2007] by estimating the soil moisture EOFs from topographic data, and *Coleman and Niemann* [2013] used a conceptual water balance called

the Equilibrium Moisture from Topography (EMT) model to downscale a catchment-wide average soil moisture to 10-40 m patterns at three catchments. In some cases, topographic downscaling methods also use other types of data. *Pellenq et al.* [2003] presented a model to downscale soil moisture to a 100 m resolution at the Nerrigundah catchment using both topographic and soil depth information. *Temimi et al.* [2010] used an index that combines topographic attributes and the leaf area index (LAI) to estimate soil moisture at a 90 m resolution. *Ranney et al.* [2015] generalized the *Coleman and Niemann* [2013] model to accept fine scale soil and vegetation data and called it the Equilibrium Moisture from Topography, Vegetation, and Soil (EMT+VS) model. Using this approach, vegetation data were found to provide more value for downscaling than soil data, particularly if the soil data are sparse or uncertain.

When any of these downscaling methods are used over large spatial extents, they must inevitably accept and downscale multiple coarse-resolution grid cells (i.e. a coarse grid of soil moisture values rather than a single average soil moisture value). Some studies have not encountered this issue because they have focused on downscaling within an area that falls within a single coarse grid cell [*Busch et al.*, 2012, *Coleman and Niemann*, 2013, *Pellenq et al.*, 2003, *Perry and Niemann*, 2007, *Ranney et al.*, 2015, *Wilson et al.*, 2005]. Other studies have downscaled multiple coarse grid values but have not considered this issue in depth. Several of these algorithms downscale each coarse grid cell independently from the adjacent coarse grids [*Fang and Lakshmi*, 2014, *Merlin et al.*, 2013, *Merlin et al.*, 2012], but the resulting soil moisture maps show unnatural discontinuities in the soil moisture values at the coarse grid boundaries. Such discontinuities might be problematic for applications like routing vehicles across the landscape [*Flores et al.*, 2014]. *Song et al.* [2014] downscaled in a way that uses

information from neighboring coarse grid values and avoids such discontinuities. Only a few studies have directly discussed the treatment of multiple coarse grid cells [Kaheil *et al.*, 2008, Kim and Barros, 2002, Sahoo *et al.*, 2013]. Kim and Barros [2002] used a sliding window to statistically downscale soil moisture and avoid the discontinuities at the boundaries. Kaheil *et al.* [2008] applied a spatial pattern search where pixels are sorted and interpolated to overcome the issue. Sahoo *et al.* [2013] used a localization radius (distance from fine grid cell being downscaled), which is a function of the spatial correlation of the errors, to determine which coarse grids affect each particular fine grid pixel. However, no studies have examined the treatment of multiple grid cells for topographically-based downscaling methods or considered how their treatment affects the downscaling performance.

The objective of this paper is to develop and test approaches for accepting multiple coarse grid cells when downscaling soil moisture. In particular, the EMT+VS model is generalized to accept multiple coarse grid cells, and approaches for treating the coarse grids are implemented and compared. The EMT+VS model is selected because it is a flexible topographically-based downscaling method. This flexibility allows it to reproduce both valley-dependent and hillslope-dependent soil moisture patterns, and it can reproduce temporally unstable soil moisture patterns [Coleman and Niemann, 2013]. It has also been shown to outperform a statistical downscaling method when calibration data are limited [Werbylo and Niemann, 2014]. The methods for accepting multiple coarse grid cells are evaluated by application to three small catchments (Tarrawarra, Cache la Poudre, and Nerrigundah) and one large region (Eastern Victoria).

2. METHODOLOGY

2.1 EMT+VS MODEL OVERVIEW

This sub-section briefly summarizes the pre-existing EMT+VS model. More details can be found in *Coleman and Niemann* [2013] and *Ranney et al.* [2015]. The EMT+VS model downscales soil moisture using a water balance of the hydrologically active soil layer. That layer begins at the ground surface and ends at the depth where the hydraulic conductivity begins to decrease significantly due to a lower permeability soil layer or bedrock. The hydrologically active layer has ranged from 5 cm and 30 cm depth in past model applications [*Ranney et al.*, 2015]. Over this range of depths, soil moisture is assumed to be constant.

Four processes are represented in the water balance: infiltration, deep drainage (or groundwater recharge), lateral flow, and evapotranspiration (ET). Each process is written as a function of topographic, vegetation, and soil characteristics. Infiltration uses the fractional vegetation cover to account for interception losses. Deep drainage is described using Darcy's Law with a percolation assumption. Lateral flow is described using Darcy's Law and assuming that the drainage area describes the contribution of flow from upslope. The lateral hydraulic gradient is estimated using a function of the topographic slope, and the soil layer thickness depends on the topographic curvature. The ET representation includes separate radiation and aerodynamic terms. Spatial variations in insolation are described using the potential solar radiation index (PSRI), which is a function of the topographic slope and aspect [*Dingman, 2002*]. The ET model also uses the fractional vegetation cover to account for the partitioning of ET into soil evaporation and transpiration and to account for shading effects on soil evaporation.

The fine-resolution soil moisture is calculated by assuming that the processes are in equilibrium. The model can still produce soil moisture that varies in time if the coarse soil moisture input varies in time, but time does not explicitly appear in the model. The equilibrium assumption disallows consideration of hysteresis in the spatial patterns of soil moisture. The equation for the fine-resolution soil moisture is a weighted average of explicit analytical solutions for the soil moisture. Each of the explicit solutions is obtained by assuming that one of the outflow terms is much larger than the others. The final equation for the fine-resolution soil moisture θ is:

$$\theta = \frac{w_G \theta_G + w_L \theta_L + w_R \theta_R + w_A \theta_A}{w_G + w_L + w_R + w_A} \quad (1)$$

where θ_G , θ_L , θ_R , and θ_A are the analytical soil moisture estimates if deep drainage, lateral flow, radiative ET, and aerodynamic ET dominate, respectively. The weights w_G , w_L , w_R , and w_A determine how important θ_G , θ_L , θ_R , and θ_A are to the final soil moisture estimate, respectively.

The deep drainage estimate of soil moisture is:

$$\theta_G = \bar{\theta} \frac{\text{DDI}}{\overline{\text{DDI}}} \quad (2)$$

where DDI is the deep drainage index, which is defined:

$$\text{DDI} \equiv \phi \left(\frac{1 - \lambda V}{K_{s,v}} \right)^{1/\gamma_v} \quad (3)$$

In these equations, $\bar{\theta}$ is the spatial-average soil moisture, $\overline{\text{DDI}}$ is the spatial average of the DDI, ϕ is soil porosity, λ is interception efficiency, V is fractional vegetation cover, $K_{s,v}$ is vertical saturated hydraulic conductivity, and γ_v is the vertical pore disconnectedness index. In

a typical application, $\bar{\theta}$ is the soil moisture that is being downscaled, V is fine-resolution vegetation cover data, and the other variables are typically either specified or calibrated constants. However, the model derivation allows all variables in Equation (3) except γ_v to vary at the fine resolution if desired [Ranney *et al.*, 2015]. The variable $\overline{\text{DDI}}$ is calculated by averaging the fine resolution data.

The lateral flow estimate of soil moisture is:

$$\theta_L = \bar{\theta} \frac{\text{LFI}}{\overline{\text{LFI}}} \quad (4)$$

where LFI is the lateral flow index, which is defined:

$$\text{LFI} \equiv \phi \left(\frac{1 - \lambda V}{\delta_0 \iota K_{s,v}} \right)^{1/\gamma_h} \left(\frac{A}{c S^\varepsilon} \right)^{1/\gamma_h} \left(\frac{\kappa_{\min}}{\kappa_{\min} - \kappa} \right)^{1/\gamma_h} \quad (5)$$

$\overline{\text{LFI}}$ is the spatial average of the LFI, A is the contributing area for the fine grid cell under consideration, δ_0 is the thickness of the soil layer where the topographic curvature is zero, ι is the anisotropy of hydraulic conductivity, c is the linear dimension of the fine grid cell, S is topographic slope, ε relates the horizontal hydraulic gradient to the topographic slope, κ_{\min} is the minimum topographic curvature that has soil present, κ is topographic curvature, and γ_h is the horizontal pore disconnectedness index. In practice, A , S , and κ are determined from the fine-resolution Digital Elevation Model (DEM) and produce spatial variations in θ_L . The other variables are typically constant (but all variables except γ_h can vary at the fine resolution if desired).

The radiative ET estimate of soil moisture is:

$$\theta_R = \bar{\theta} \frac{\text{REI}}{\overline{\text{REI}}} \quad (6)$$

where REI is the radiative ET index, which is defined:

$$\text{REI} \equiv \phi \left\{ \frac{1+\alpha}{E_p} \right\}^{1/\beta_r} \left(\frac{1}{I_p} \right)^{1/\beta_r} \left[\frac{(1-\lambda V)}{\eta V + (1-V)^\mu} \right]^{1/\beta_r} \quad (7)$$

$\overline{\text{REI}}$ is the spatial average of the REI, α is the ratio of aerodynamic to radiative ET (i.e. the Priestly-Taylor coefficient minus one), E_p is the average potential ET, I_p is the PSRI, η is the portion of transpiration that is met by the modeled soil layer, μ describes the effect of shading on soil evaporation, and β_r is the radiative ET exponent. In practice, spatial variations in θ_R are produced by I_p , which is determined from the fine-scale DEM, and V . The other variables are typically constant (but all variables except β_r can vary at the fine resolution if desired).

The aerodynamic ET estimate of soil moisture is:

$$\theta_A = \bar{\theta} \frac{\text{AEI}}{\overline{\text{AEI}}} \quad (8)$$

where AEI is the aerodynamic ET index, which is defined:

$$\text{AEI} \equiv \phi \left\{ \frac{1+\alpha}{\alpha E_p} \right\}^{1/\beta_a} \left[\frac{1-\lambda V}{\eta V + (1-V)^\mu} \right]^{1/\beta_a} \quad (9)$$

$\overline{\text{AEI}}$ is the spatial average of the AEI and β_a is the aerodynamic ET exponent. In practice, V produces variations in θ_A and all other variables in Equation (9) are typically constants (but the derivation allows all variables except β_a to vary at the fine resolution if desired).

The weights are calculated from the magnitudes of the outflow terms in the water balance equation and are calculated as:

$$w_G = \left(\frac{\bar{\theta}}{\overline{\text{DDI}}} \right)^{\gamma_v} \quad (10)$$

$$w_L = \left(\frac{\bar{\theta}}{\overline{\text{LFI}}} \right)^{\gamma_h}, \quad (11)$$

$$w_R = \left(\frac{\bar{\theta}}{\overline{\text{REI}}} \right)^{\beta_r}, \quad (12)$$

and:

$$w_A = \left(\frac{\bar{\theta}}{\overline{\text{AEI}}} \right)^{\beta_a} \quad (13)$$

Because the exponents in the weight equations are all required to be spatially constant, the weights also are spatially constant in the EMT+VS model.

2.2 GENERALIZATION TO MULTIPLE COARSE GRID CELLS

All previous applications of the EMT+VS model downscaled a single spatial-average soil moisture ($\bar{\theta}$) at any given time, which implies that single values were used for $\overline{\text{DDI}}$, $\overline{\text{LFI}}$, $\overline{\text{REI}}$, and $\overline{\text{AEI}}$. The EMT+VS model can accept multiple coarse grid cells without any revision to the model derivation. In this case, the spatial-averages ($\bar{\theta}$, $\overline{\text{DDI}}$, $\overline{\text{LFI}}$, $\overline{\text{REI}}$, and $\overline{\text{AEI}}$) have multiple values over the region of interest. However, to obtain these averages, one needs to select the spatial extent over which the averages are calculated (referred herein as the window) and how the data within the window are used to calculate the averages (i.e. the data weighting).

Two windowing methods are considered in this paper (fixed and shifting). The fixed window (**Figure 1a**) calculates the spatial averages over the same spatial extents as the coarse grid cells of soil moisture. Thus, every fine grid cell within a given coarse grid cell has the same window and thus the same values for $\bar{\theta}$, $\overline{\text{DDI}}$, $\overline{\text{LFI}}$, $\overline{\text{REI}}$, and $\overline{\text{AEI}}$. The fixed window is a direct extension of the previous applications of the EMT+VS model because each coarse grid

cell is downscaled independently. This windowing method is analogous to the approaches used by *Fang and Lakshmi* [2014], *Merlin et al.* [2013], and *Merlin et al.* [2012]. The shifting window (**Figure 1b**) has the same size as the coarse grid cells of soil moisture, but it is always centered on the fine grid cell that is being calculated. Thus, every fine grid cell can have different values of $\bar{\theta}$, \overline{DDI} , \overline{LFI} , \overline{REI} , and \overline{AEI} , and these values can depend on multiple coarse grid cells. This windowing method is similar to the approaches used by *Song et al.* [2014], *Kaheil et al.* [2008], *Kim and Barros* [2002], and *Sahoo et al.* [2013].

Once the window extent is determined, the averages must be calculated using the data within the window. The fixed window always aligns with the coarse soil moisture grid, so $\bar{\theta}$ is simply the soil moisture value for that coarse grid cell. Due to their definitions in the model derivation, \overline{DDI} , \overline{LFI} , \overline{REI} , and \overline{AEI} must be calculated in a manner consistent with $\bar{\theta}$, so they are found using an arithmetic average of the values within the fixed window (those variables are calculated using the fine-resolution data). This approach implicitly assumes that the coarse soil moisture values equally weight all soil moisture values that occur within the coarse grid cell. This assumption might be violated for some remote sensing products. In contrast, the shifting window typically includes multiple coarse grid cells, so $\bar{\theta}$ must be calculated. To obtain $\bar{\theta}$, a fine grid is filled with the coarse soil moisture values as shown in **Figure 1b**. Then, the weight for each fine grid cell in the window is calculated using the distance of the fine grid cell from the window center (i.e. where the local soil moisture is being calculated). Three weighting schemes are considered (box, disk, and Gaussian). Box weighting has the same window size and shape as the coarse grid cells (i.e. rectangular or square), and each fine grid cell within the window is weighted equally (**Figure 1c**). It is equivalent to the weighting used by the fixed window method. Disk weighting has equal weights within a circle

whose area is equal to the coarse grid area (**Figure 1d**). Gaussian weighting uses a window whose radius is 3σ (where σ is a parameter). Within the window, the weights are found from a Gaussian probability density function with standard deviation σ (**Figure 1e**).

3. APPLICATION TO TEST SITES

3.1 TEST SITE PROPERTIES

The generalized EMT+VS model is tested by application to three small catchments and one large region. The three catchments are the same ones considered by *Ranney et al.* [2015]. They are used here because they have nearly complete grids of high-quality local soil moisture observations. Thus, the coarse grid cells can have nearly any size and position and still contain soil moisture observations that can be used to evaluate the model performance. Unfortunately, due to the small extents of these catchments, the coarse grid cells must be much smaller than those produced by satellites. Thus, we also analyze one large region. This region does not have local soil moisture observations, but large coarse grid cells can be used (the output from a land surface model) and the different methods for treating multiple coarse grid cells can still be compared.

The Tarrawarra catchment was originally described by *Western and Grayson* [1998] and is located in Victoria, Australia (37°39'S, 145°26'E). The catchment is 10.5 ha. A 5 m DEM is available and was originally developed using a total station survey (**Figure 2a**). Topographic relief is 25 m. Tarrawarra has a temperate climate with an average annual rainfall of 820 mm and an average annual potential evapotranspiration (PET) of 830 mm. The vegetation is grazed pasture. The soil moisture dataset was collected using time domain reflectometry (TDR) and includes thirteen dates spanning fourteen months (from 27 Sept 95 to 29 Nov 96). The measurements characterize the top 30 cm of the soil at a 10 m by 20 m spacing.

The Nerrigundah catchment is located near Dungog, Australia (32°19'S, 151°43'E) and is described in detail by *Walker et al.* [2001]. It has an area of 6 ha. A 20 m DEM is available

and was originally developed using a total station (**Figure 2b**). Topographic relief is 27 m. Nerrigundah has a temperate climate with an average annual precipitation of 1000 mm and a class A pan evaporation of 1600 mm. The vegetation is predominately grasses. The soil moisture dataset was collected using TDR and consists of twelve dates over two months (27 Aug 97 to 22 Sept 97). The measurements characterize the top 15 cm of the soil at a 20 m by 20 m grid spacing.

The Cache la Poudre catchment is located near Rustic, Colorado ($40^{\circ}41'57''\text{N}$, $105^{\circ}30'25''\text{W}$) and is described by [Coleman and Niemann, 2012]. It is approximately 8 ha. A 15 m DEM is available and was developed using a total station and survey-grade global positioning system (**Figure 2c**). Topographic relief is 124 m. The catchment has a semiarid climate with an average annual precipitation of 400 mm and an average annual PET of 930 mm. The vegetation is aspect dependent with shrubs on the south-facing hillslopes and coniferous trees on the north-facing hillslopes. Unlike the other catchments, data are available to describe the fractional vegetation cover on a 15 m by 15 m grid. These data were originally generated using a multispectral digital camera and manual measurements of litter depth as described by Ranney *et al.* [2015]. Soil moisture was observed using a TDR on nine sampling dates over three months (21 Apr 08 to 24 Jun 08). The measurements characterize the top 5 cm of the soil at a 15 m by 15 m grid spacing.

Eastern Victoria is a large region that surrounds the Tarrawarra catchment ($37^{\circ}48'55''\text{S}$ to $36^{\circ}57'02''\text{S}$, $145^{\circ}07'23''\text{E}$ to $145^{\circ}59'13''\text{E}$). The region has an area of 7575 km². A 30 m DEM is available from the Advanced Spaceborne Thermal Emission and Reflection Radiometer (ASTER) [Hirano *et al.*, 2003, Yamaguchi *et al.*, 1998] (**Figure 2d**). The region has 1,493 m

total relief and varies from forested mountains in the east to agricultural plains in the west. No local soil moisture observations are available to evaluate the downscaling model's performance.

3.2 MODEL APPLICATION

For Tarrawarra, Nerrigundah, and Cache la Poudre, the coarse soil moisture inputs were determined by averaging the local observations within the coarse grid cells of the selected size and position. The model parameters were calibrated using the same procedure described by *Ranney et al.* [2015]. Specifically, the parameter ranges were constrained using the available soil, vegetation, and climatic information. Then, final parameter values were selected to maximize the average Nash Sutcliffe Coefficient of Efficiency (NSCE) [*Nash and Sutcliffe*, 1970] among all days in the catchment's dataset. NSCE is applied spatially by taking differences between EMT+VS estimates and the measured soil moisture at each point. Spatial NSCE values for each sampling data are then averaged arithmetically over all dates.

For Eastern Victoria, a coarse grid of soil moisture is available from the Agricultural Meteorology model (AGRMET). AGRMET is a global land surface model from the Air Force Weather Agency (AFWA) that produces satellite-based radiation and precipitation products [*AFWA*, 2002]. The dataset consists of six dates spanning seven months (15 Mar 08 to 31 Oct 08). The dates were selected to capture a wide range of moisture conditions. The dataset characterizes the top 10 cm of the soil and includes sixteen coarse grid cells within the region. The Data Processing and Error Analysis System (DPEAS) [*Jones and Vonder Haar*, 2002] was used for spatial remapping, and the data were then projected to obtain grid cells that are roughly 19 km by 24 km. Although the grid cells are not exactly rectangular, after projection they were approximated as rectangular for simplicity of testing. Nearly all parameters for Eastern Victoria

were taken directly from Tarrawarra without additional calibration. These parameters may be applicable for the agricultural region near Tarrawarra but are likely inaccurate for other dissimilar portions of the region. Nonetheless, they are the best available parameters for this region and provide representative soil moisture patterns for testing. Only the anisotropy ι was changed (from 47.2 to 250) so that the downscaled soil moisture map more consistently produced saturation at locations where streams are observed in satellite photos of the region.

4. RESULTS AND DISCUSSION

We begin by evaluating the accuracy of the fixed window procedure when it is applied to the three catchments and different coarse grid cell sizes are used (**Figure 3**). For this test, the EMT+VS model was applied using two calibration approaches (single and repeated). For single calibration, the parameters for each catchment were determined when the model was supplied with a single coarse soil moisture value as input (the same scenario considered by *Ranney et al.* [2015], see **Appendix A**). These parameters were then used for all coarse grid cell sizes. For repeated calibration, the parameters were recalibrated for each coarse grid cell case. For each coarse grid cell size, a collection of grids was generated using all possible grid origins (i.e. grid positions). The NSCE values shown in **Figure 3** are the averages among all dates in the dataset and among all origins for the given cell size. The sizes of the coarse grid cells were determined using a constant increment in their linear dimension (e.g., 20 m). However, due to the irregular boundaries of the catchments, the available soil moisture measurements do not necessarily span the full extent of a specified coarse grid cell. For example, if a single very large grid cell were specified, the average soil moisture for that cell could only be calculated from measurements within the catchment area. Thus, an effective cell size was calculated as the average area that is characterized by the measurements in each grid cell, and the square root of the effective cell size is used as the abscissa in **Figure 3**.

The NSCE of the fine-resolution soil moisture that is produced by the fixed window procedure can be compared to the NSCE of the coarse resolution input. If the input is a single value (i.e. one large coarse grid cell is used), then the NSCE of the input is zero (beyond the right edge of the plots in **Figure 3**) because none of the spatial variability is captured and the mean

value is preserved. However, as the coarse grid becomes finer (shifting to the left in **Figure 3**), more variability is captured before downscaling and the NSCE of the input increases. **Figure 3** shows that the output from the fixed window method also captures more variability as the coarse grid becomes finer. This result shows that the downscaling model benefits from the additional information that is provided by the higher resolution input. The NSCE of the fixed window output is also greater than the coarse input NSCE for all resolutions considered, which suggests that the downscaled pattern reproduces additional spatial variability even when relatively fine grid cells are supplied as input. However, the difference between the input and output NSCE values becomes smaller as the coarse resolution input becomes finer. Thus, downscaling provides less incremental benefit when the coarse resolution input is already capturing much of the spatial variation. The difference in performance between the single and repeated calibrations is consistently small (about 0.02 on average), which suggests that the parameter values are not strongly dependent on the resolution of the soil moisture input and are relatively robust at each catchment. The difference grows slightly as the coarse grid becomes finer because the single calibration is performed with a large effective grid cell size (i.e. one cell). Single calibration is used in all the remaining analyses.

Figure 4 shows the coarse input, output soil moisture, and the observed soil moisture patterns for one date at Tarrawarra when different resolutions are used for the input. The day shown (27 Sep 95) has intermediate soil moisture among those in the dataset. The observed pattern (repeated in **Figures 4g-i**) exhibits the wettest conditions in the valley bottoms, moderate moisture on the south-facing hillslope, and the driest conditions on the north-facing slope. The coarse-resolution inputs (**Figure 4a-c**) provide better information about the soil moisture pattern as the resolution improves from 220 m to 100 m. In particular, the finer resolutions begin to

capture the difference in moisture between the opposing hillslopes, but the wet valley bottoms are not captured. The soil moisture patterns from the EMT+VS model reproduce the main features in the observed patterns but underestimate the overall range in moisture values. The difference in moisture between the opposing hillslopes is better captured as the resolution of the input improves. The EMT+VS soil moisture patterns also exhibit abrupt changes in moisture at the boundaries of the coarse grid cells. These features occur because each coarse grid cell is independently downscaled when the fixed window procedure is used. They are also similar to the abrupt changes observed for other methods that downscale each cell independently [Fang and Lakshmi, 2014, Merlin et al., 2013, Merlin et al., 2012].

The accuracy of the fixed window procedure is compared to that of the shifting window procedure in **Figure 5**. The analysis was performed in the same manner as **Figure 3**, but the shifting window procedure was implemented with box, disk, and Gaussian weighting. For Gaussian weighting, σ was selected to be the length of the coarse grid cell (Δx) divided by 2.35. This σ value makes the weight at the edge of the window half of the weight at the center of the window. For all catchments and coarse resolutions considered, the fixed window procedure has higher average NSCE values than the shifting window procedure (on average, it is about 0.03 higher). However, the performance of the two methods becomes more similar as the resolution gets coarser (particularly at Tarrawarra where the two methods converge). The performance of the fixed and shifting window methods were also evaluated using root-mean squared error (RMSE) and mean relative error (MRE) and similar results to NSCE were found. On average, the RMSE of the fixed window procedure is about $0.00074 \text{ m}^3 \text{ m}^{-3}$ lower than that of the shifting window procedure. Similarly, the MRE is about 0.0063 smaller for the fixed window procedure. The weighting method has only a small effect on the performance of the shifting

window procedure, and the method with the best performance differs between catchments (**Figure 5**). For Tarrawarra and Cache la Poudre, Gaussian weighting usually performs the best, but for Nerrigundah, it usually performs the worst.

One reason that the fixed window procedure outperforms the shifting window procedure can be seen in **Figure 6**. Results in **Figure 6** consider the RMSE (m^3m^{-3}) of the average soil moisture that is calculated from the output fine-resolution pattern within each coarse grid cell. The fixed window procedure always has zero RMSE because it maintains the average soil moisture in each coarse grid cell exactly. The fixed window always aligns with the coarse grid, so the coarse soil moisture value is directly used in the downscaling method. The shifting window procedure does not preserve the average soil moisture in each coarse grid cell because the window is centered on the fine grid cell of interest and the average is usually calculated from multiple adjacent coarse grid values. The RMSE of the average soil moisture is typically about 0.02, 0.05, and 0.08 m^3m^{-3} for the Tarrawarra, Nerrigundah, and Cache la Poudre catchments, respectively. These errors do not change significantly with resolution. The differing RMSE values are likely due to differences in the spatial correlation structure of the observed soil moisture. This error is a key reason why the shifting window procedure is less accurate than the fixed window procedure. It also suggests that the fixed window procedure is likely to perform better than the shifting window procedure if used in other downscaling methods because the same situation would occur.

Figure 7 shows example output soil moisture maps for Nerrigundah when the fixed window and shifting window procedures (with associated weighting methods) are used. The day shown (15 Sep 97) has intermediate soil moisture relative to the rest of the dataset. Similar to **Figure 4**, the fixed window procedure produces abrupt changes in moisture at the coarse grid

boundaries (**Figure 7c**). In contrast, all three shifting window procedures produce smooth transitions at these boundaries (**Figure 7d-f**). The soil moisture maps produced by the three weighting procedures (box, disk, and Gaussian) are similar in appearance just as they were similar in accuracy. The generated soil moisture patterns from the other dates and catchments showed similar results.

Gaussian weighting differs from the other procedures because it requires specification of a parameter σ . **Figure 8** shows the performance of the downscaling method when three different values of σ are used: $\Delta x/2.35$, $\Delta x/4$, and $\Delta x/6$. Larger sigma values were also tested but do not perform better than those shown in **Figure 8**. For $\sigma = \Delta x/4$, 95% of the overall weight is given to points within a distance of Δx . Likewise, $\sigma = \Delta x/4$ creates a window with 99.7% of the weight falling within the distance of Δx . For reference, the NSCE for the fixed window procedure is also included in **Figure 8**. The best σ value is inconsistent between different catchments and resolutions. While $\sigma = \Delta x/2.35$ is usually the most accurate Gaussian procedure at Tarrawarra and Cache la Poudre, it is the least accurate at Nerrigundah. Also, the best σ value depends on the coarse grid resolution at Cache la Poudre, with the best value changing at a resolution near 36 m. These inconsistencies are again likely due to differences in the spatial correlation structure of the soil moisture and the EMT+VS indices at each catchment.

Next, we evaluate the downscaling methods for the large Eastern Victoria region, which allows consideration of much larger coarse grid cells. Because local soil moisture observations are not available to evaluate the model results, we assume that the fixed window procedure remains the most accurate for this large region and evaluate the difference between the other methods and the fixed window method. **Figure 9** shows the NSCE for the shifting window

procedure (with different weighting methods) when compared to fixed window procedure.

Specifically, **Figure 9a** shows this NSCE for the small Tarrawarra catchment when a range of coarse grid resolutions are used, and **Figure 9b** shows this NSCE for the large Eastern Victoria region when the coarse resolution AGRMET data are used. The high NSCE values in **Figure 9a** suggest that the box, disk, and Gaussian procedures are close approximations of the fixed window procedure and that the similarity increases as the size of the coarse-grid cells increases. **Figure 9b** is consistent with this trend. The similarity between the results is even higher when the very large grid cells are used across the larger region. Because of the high similarity between the fixed and shifting window patterns, the shifting window method is expected to have similar accuracy to the fixed window pattern when applied at large scales. This similarity is also confirmed when using other measures. The RMSE and MRE range 0.017-0.018 m^3m^{-3} and 0.046-0.057, respectively.

Soil moisture maps produced by the EMT+VS model for Eastern Victoria on a date with intermediate moisture (01 Nov 08) are shown in **Figure 10** (zoomed-in images are in **Appendix B**). Similar to the small catchments, the fixed window procedure produces abrupt changes in soil moisture at the coarse grid boundaries, but smooth transitions are seen for the box, disk, and Gaussian procedures. The patterns from the three shifting window procedures are almost indistinguishable visually. It should be noted that the figure shows fine resolution patterns over very large regions, so much of the variability that is introduced by downscaling is not visible here. The difference map shows the box weighting results minus the fixed window results. The largest differences are observed at the coarse grid edges. In addition, some stream patterns are evident in the differences. Near the coarse grid boundaries, the spatial averages used by the shifting window diverge from those used by the fixed window. The different averages can

produce different weighting of the underlying soil moisture estimates that are used in the EMT+VS model. Overall, the range of differences indicate that the methods produce very similar results over most areas. Maps of the box, disk, and Gaussian weighting results were also examined and appear visually indistinguishable.

Histograms of soil moisture were calculated to understand the difference in the statistical properties of the downscaled patterns. **Figure 11** shows the histograms of the input, fixed window procedure, and shifting window procedure with box weighting for the same date that was shown in **Figure 10**. The histogram of the input soil moisture (**Figure 11a**) is unrealistic (e.g., no values near 0.1 are observed) due to the coarse resolution of the map. Both downscaled soil moisture maps exhibit more continuous ranges of moisture than the input. The histograms from the fixed and shifting window (**Figure 11b-c**) procedures are similar, but the shifting window histogram has more values near 0.1. These values are associated with the smooth transition between adjacent dry and wet coarse grid cells.

Semi-variograms were also used to characterize the spatial correlation structures of the soil moisture estimates produced by the different methods. The nugget, sill, and range are all similar among the different methods, showing that spatial structures of the estimates are similar. Although the abrupt boundaries between large cells are visually pronounced, the boundary area is very small compared with the domain, so the nugget effect is reduced by pairs away from the boundary. Differences over short lags are also dominated by stream channels in both methods. In a further attempt to see a statistical difference in the nugget, the boundaries were isolated (points far from boundaries were removed) and the new images were analyzed. Semi-variograms were fitted to images that included 100%, 43%, 21%, and 8.5% of Eastern Victoria by area as seen in **Appendix C**. At 43% area, the fixed method had a nugget of 0.00166 and box

weighting had a nugget of 0.00154. Other areas that were analyzed had nuggets that were the same for the fixed method and box weighting.

It is worth noting that the computational efficiency varies for the different weighting methods. The fixed window procedure is much quicker than the shifting window procedure because each coarse grid cell is downsampled independently and can be processed in parallel. For the shifting window procedure, box weighting is the most efficient because it utilizes two 1-D filters that are the same length and width as the coarse grid. The 1-D filter is passed over the image twice (once vertically and once horizontally) producing the equivalent of a 2-D filter. Gaussian weighting also utilizes the two 1-D filters, but it is slightly more computationally expensive than box weighting because the window is typically larger (due to the tail on the Gaussian distribution). Disk weighting is much more computationally expensive because it cannot easily utilize the 1-D filter algorithm. It requires about ten times the computation time of the other shifting window methods.

5. CONCLUSIONS

In this paper, the EMT+VS model was generalized to downscale soil moisture from multiple coarse resolution grid cells. The presence of multiple grid cells affects the calculation of spatial averages that appear in the EMT+VS model. To calculate these averages, two windowing methods were considered (fixed and shifting), and for the shifting window, three weighting methods were evaluated (box, disk, and Gaussian). Based on the results, the following conclusions can be made:

1. The EMT+VS model successfully downscales soil moisture when supplied with multiple coarse-resolution grid cells of soil moisture. Specifically, for all catchments and coarse resolutions considered, the soil moisture patterns produced by the model capture more of the observed soil moisture variability than the coarse grid soil moisture patterns, which suggests that the downscaling provides added value. The accuracy of the generated soil moisture patterns improves as the resolution of the coarse grid becomes finer. However, the increase in the NSCE compared to the coarse resolution input becomes smaller as the coarse grid becomes finer. The calibrated parameter values are also relatively robust with respect to the resolution of the input.
2. Among the two windowing methods considered, the fixed window method provides the more accurate fine-resolution soil moisture patterns. The NSCE of the fixed window procedure is about 0.03 more (explains 3% more of the variance) than shifting window procedure for the small catchments. If applied to regions with larger coarse grid cells, the difference in accuracy is likely smaller because the fixed and shifting window patterns become more similar in such cases. The fixed window approach is more accurate

because it preserves the spatial average soil moisture within the original coarse grid cells. Thus, this windowing method is also expected to have better performance when used with other soil moisture downscaling methods.

3. Although less accurate, the shifting window procedure provides smooth transitions in the soil moisture between coarse grid cells for all weighting methods considered. Smooth transitions are also expected to occur if the shifting window method is used with other soil moisture downscaling methods. Smooth transitions may be important for some applications such as determining optimal vehicle routing across the landscape.
4. For the shifting window procedure, the box, disk, and Gaussian weighting methods perform similarly. The most accurate weighting method varies among the cases considered, and the best standard deviation for Gaussian weighting also depends on the case considered. In the end, the box method is recommended for practical applications because it is the most computationally efficient and does not require specification of a parameter.

Future research should consider the performance of these methods when applied to larger regions with abundant local soil moisture observations. This study evaluated the treatment of multiple coarse grid cells when those cells were relatively small due to the limited spatial extent of the available soil moisture datasets. One could instead compare against remotely-sensed estimates of soil moisture (such as AirMoss [*Chapin et al.*, 2012, *Tabatabaenejad et al.*, 2015]). Although such estimates are likely less reliable than TDR measurements, that approach would allow consideration of much larger spatial extents. The methods could also be tested when they are coupled with other soil moisture downscaling methods or when downscaling other variables. Finally, the coarse resolution soil moisture values used in our experiments were calculated as

arithmetic averages of the soil moisture values occurring within each grid cell. However, some remote sensing methods may emphasize soil moisture values that occur near the center of the coarse grid cell. The methods considered in this paper could be tested when unequal weightings are used to determine the coarse grid cell values. Likewise, further research could investigate how errors in the coarse resolution soil moisture propagate to the fine resolution soil moisture patterns.

6. FIGURES

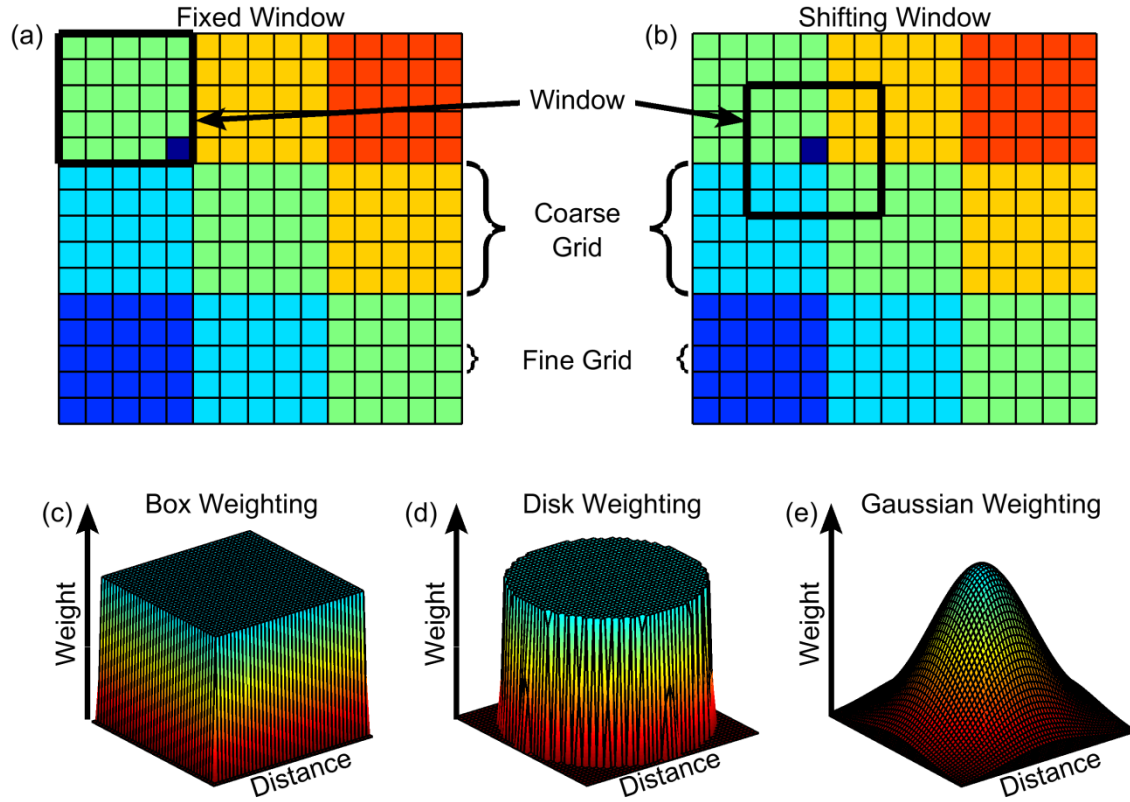


Figure 1. Illustration of the alignment of (a) the fixed window and (b) the shifting window relative to the coarse grid of soil moisture. The window determines the values that are used to calculate averages in the EMT+VS model. Also, illustration of (c) box, (d) disk, and (e) Gaussian weighting functions that are used to calculate the averages.

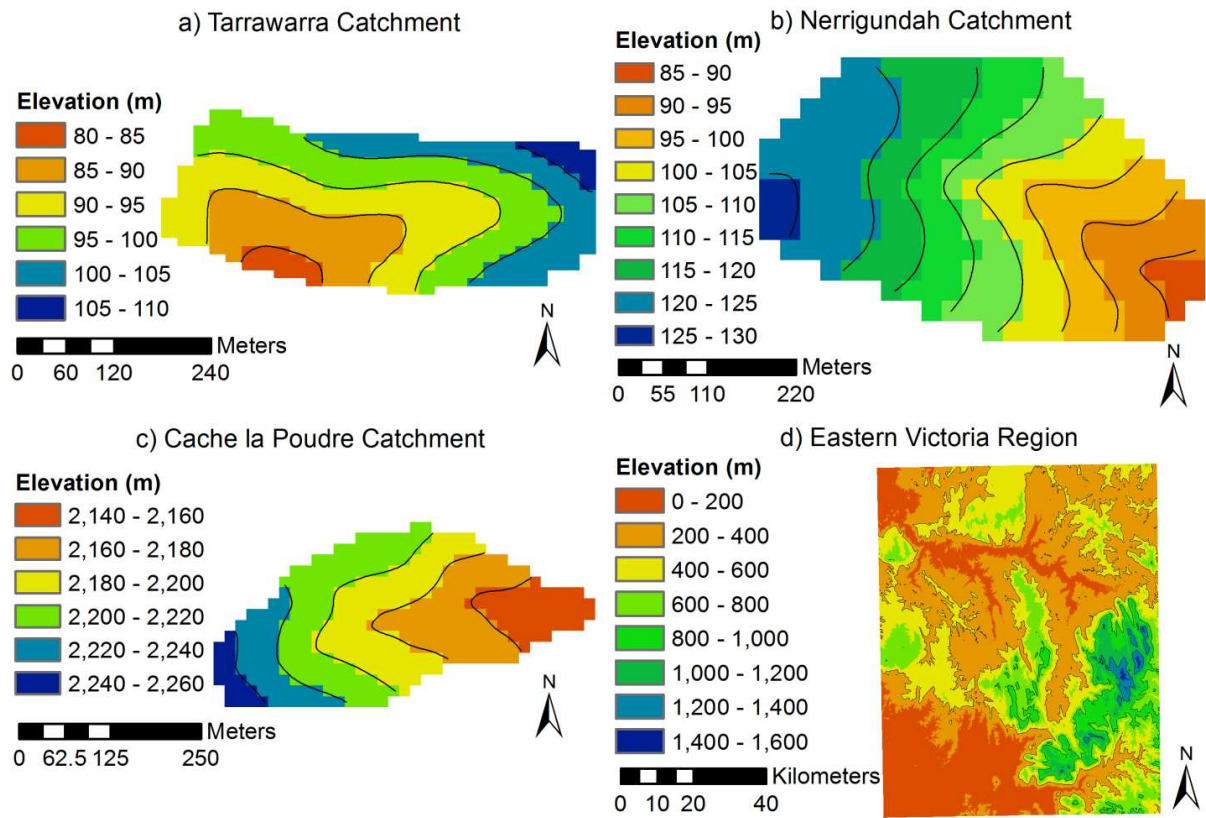


Figure 2. Topographic maps of the four test sites including (a) the Tarrawarra catchment, (b) the Nerrigundah catchment, (c) the Cache la Poudre catchment, and (d) the Eastern Victoria region (which includes the Tarrawarra catchment).

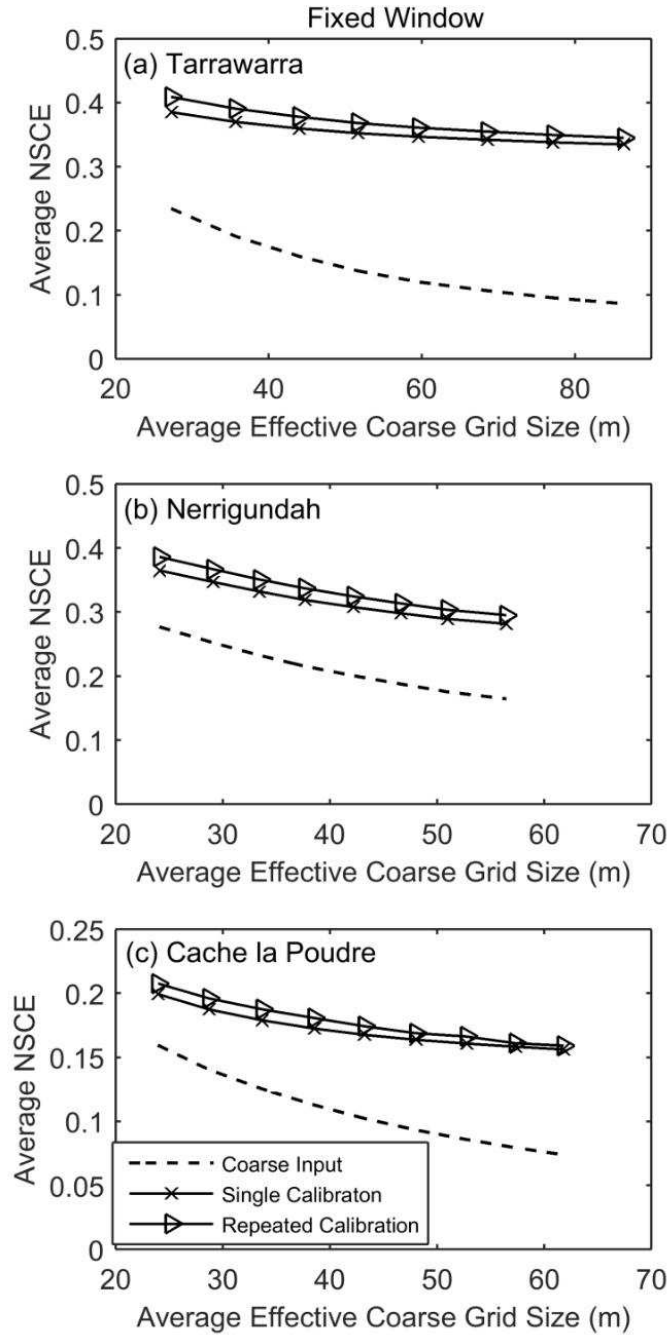


Figure 3. Evaluation of the accuracy of downscaling multiple coarse grid cells of soil moisture with the EMT+VS model when the fixed window procedure is used for (a) Tarrawarra, (b) Nerrigundah, and (c) Cache la Poudre. Average NSCEs are calculated by comparing the downscaled soil moisture to the observed soil moisture for all dates in the available dataset and all possible origins for the coarse resolution input. Average effective linear grid size refers to the resolution of the coarse grid that is supplied to the downscaling method.

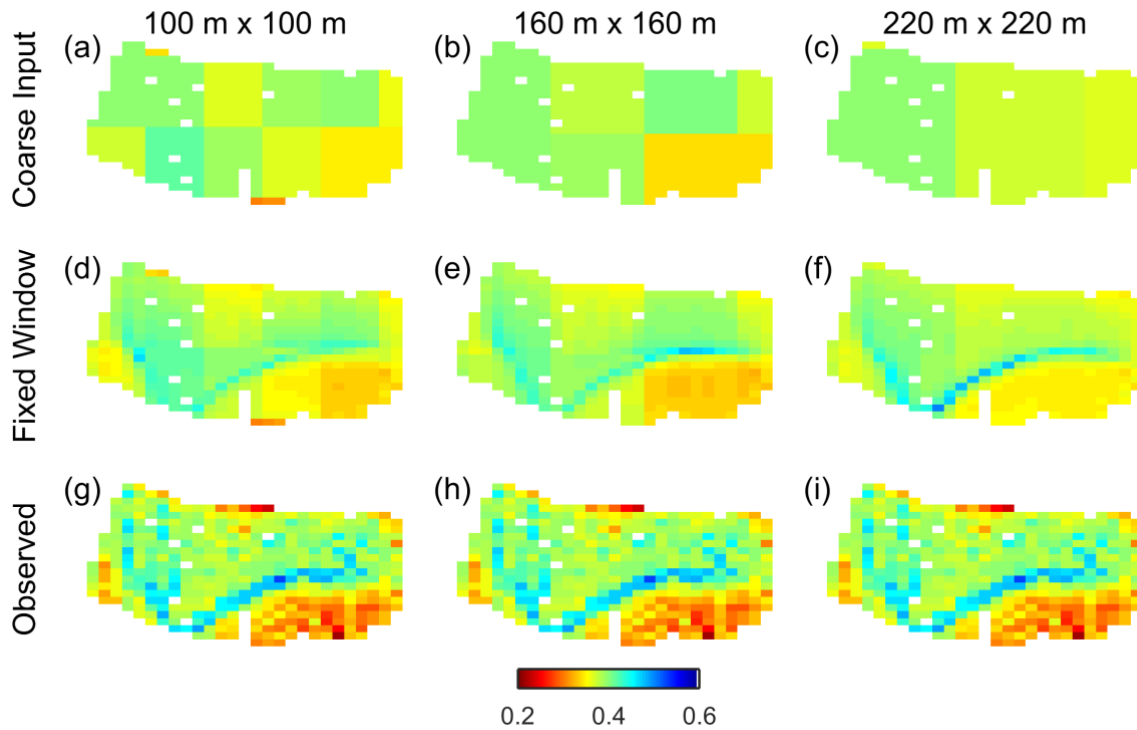


Figure 4. Soil moisture maps for Tarrawarra on 27 Sep 95. Top row (a-c) shows the coarse resolution soil moisture input (resolution becomes coarser to the right as labeled). These grid cells correspond to 74 m, 102 m, and 124 m average effective grid sizes (from left to right). Second row (d-f) shows the fine resolution soil moisture output using the fixed window procedure, and bottom row (g-i) shows the observed soil moisture (plots g-i are the same). White cells are locations with missing data.

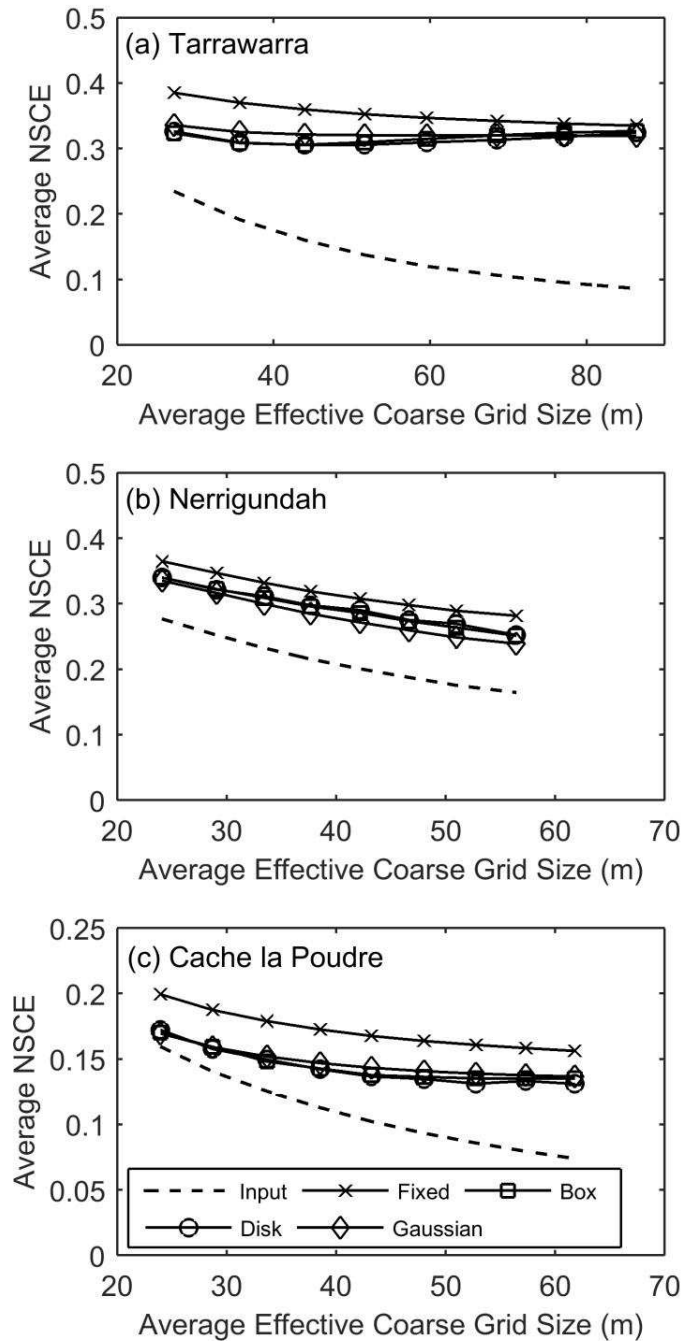


Figure 5. Comparison of the accuracy of fine-resolution soil moisture maps produced by the EMT+VS model when the fixed and shifting window procedures are used for (a) Tarrawarra, (b) Nerrigundah, and (c) Cache la Poudre. For the shifting window procedure, box, disk, and Gaussian ($\sigma = \Delta x / 2.35$) weighting are used as labeled. Average NSCEs are calculated from all dates in the available dataset and all possible origins for the coarse resolution soil moisture input.

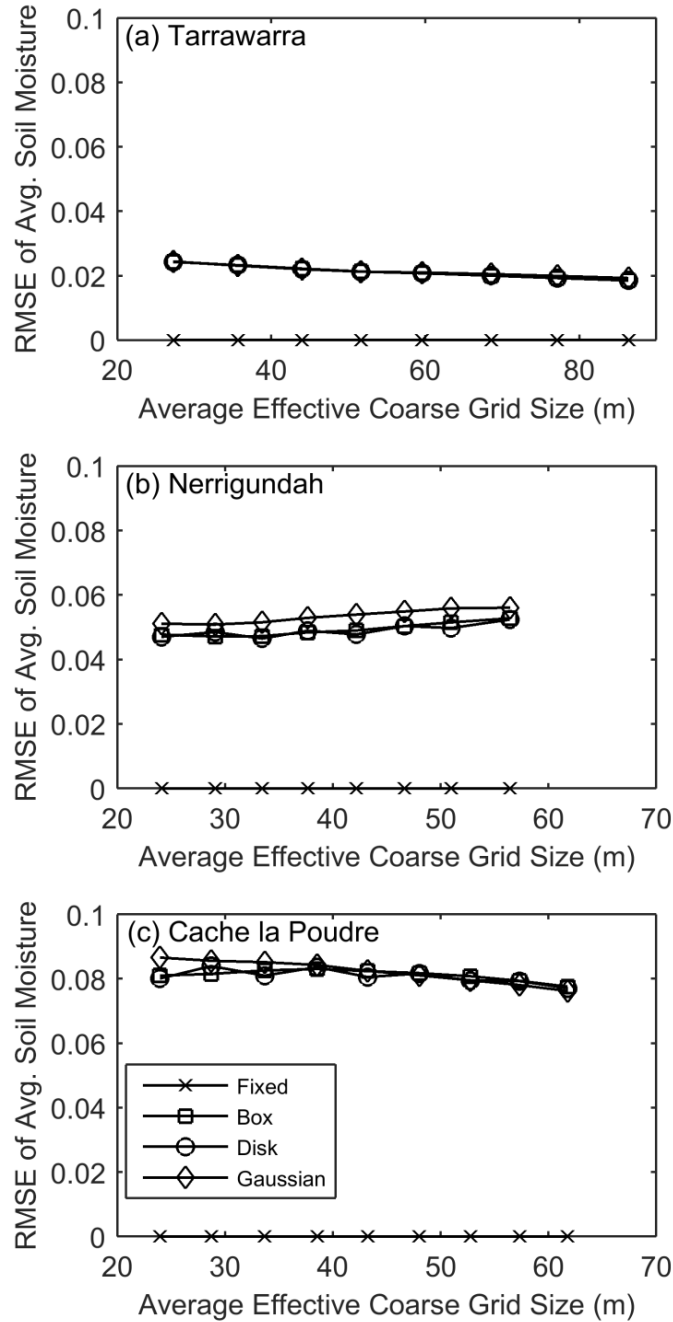


Figure 6. RMSE (m^3m^{-3}) in the average soil moisture within each coarse grid cell from the fine-resolution maps at (a) Tarrawarra, (b) Nerrigundah, and (c) Cache la Poudre. Gaussian weighting uses $\sigma = \Delta x / 2.35$. RMSEs are averages from all dates in the available dataset and all possible origins for the coarse resolution input.

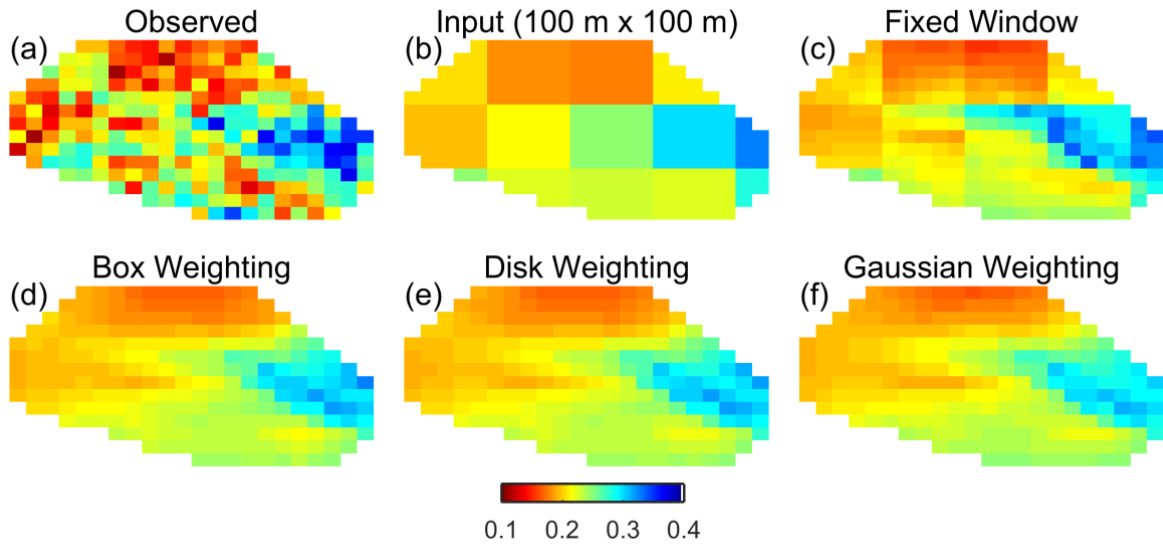


Figure 7. Soil moisture maps for 15 Sep 97 at Nerrigundah showing (a) the observed pattern, (b) the coarse resolution input (average effective grid size of 78 m), (c) the fine resolution output from the fixed window procedure, and the fine resolution output from the shifting window procedure when (d) box, (e) disk, and (f) Gaussian weighting are used. Gaussian weighting uses $\sigma = \Delta x / 2.35$.

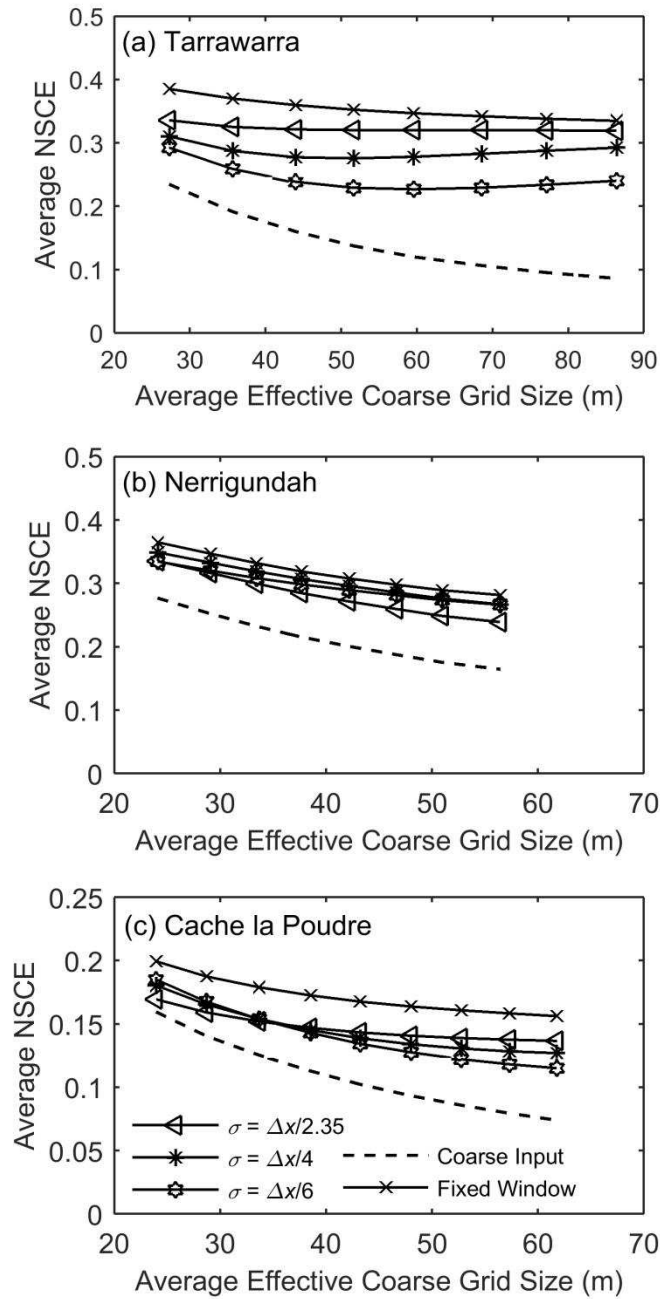


Figure 8. Comparison of the accuracy of the fine resolution soil moisture maps produced by the EMT+VS model when the shifting window procedure is used with Gaussian weighting for (a) Tarrawarra, (b) Nerrigundah, and (c) Cache la Poudre. Average NSCEs are calculated from all dates in the available dataset and all possible origins for the coarse resolution input.

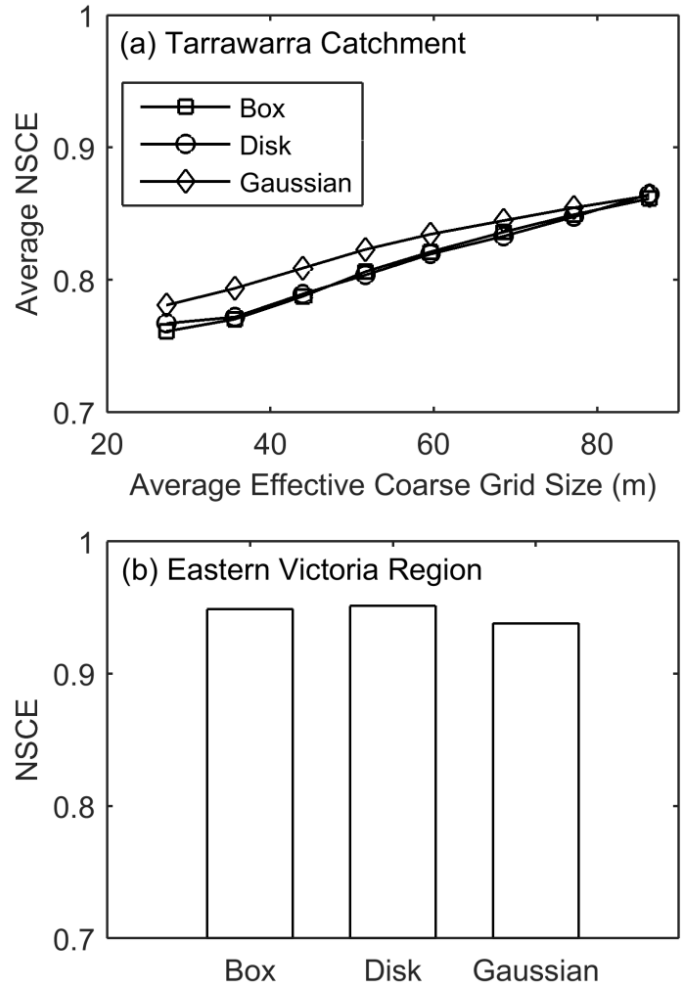


Figure 9. Similarity between the fine resolution soil moisture maps produced by the fixed and shifting window procedures at (a) the Tarrawarra catchment and (b) the Eastern Victoria region. Gaussian weighting uses $\sigma = \Delta x / 2.35$. NSCE is calculated by considering the fixed window soil moisture as the observation dataset and the other methods as the model output. For (a), average NSCEs are calculated from all dates in the available dataset and all possible origins for the coarse resolution input. For (b), only the AGRMET coarse resolution input is used.

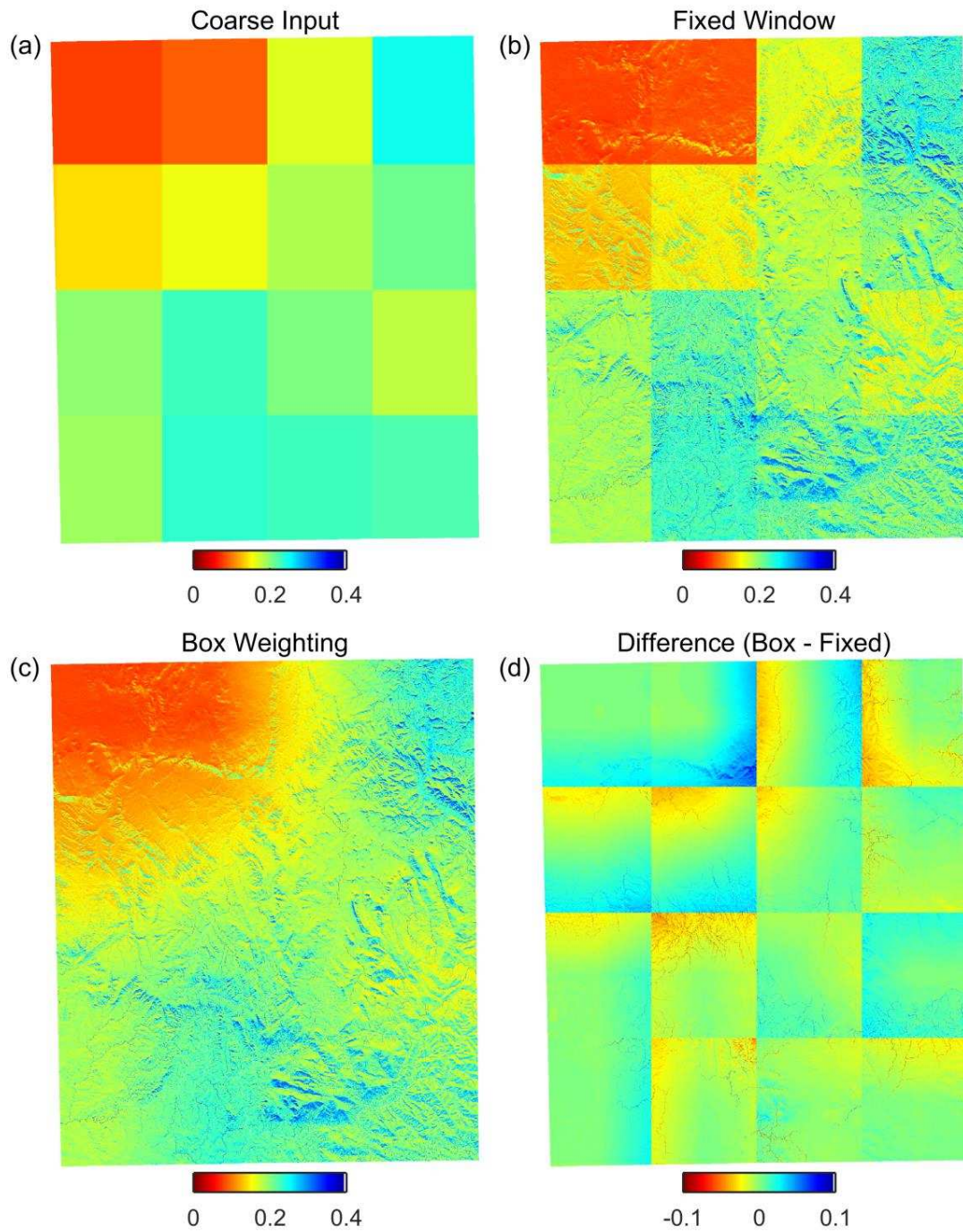


Figure 10. (a) Coarse resolution AGRMET soil moisture, (b) results of the fixed window method, (c) results of the box weighting method, and (d) results of the box weighting method minus the results of the fixed window method for Eastern Victoria on 01 Nov 08.

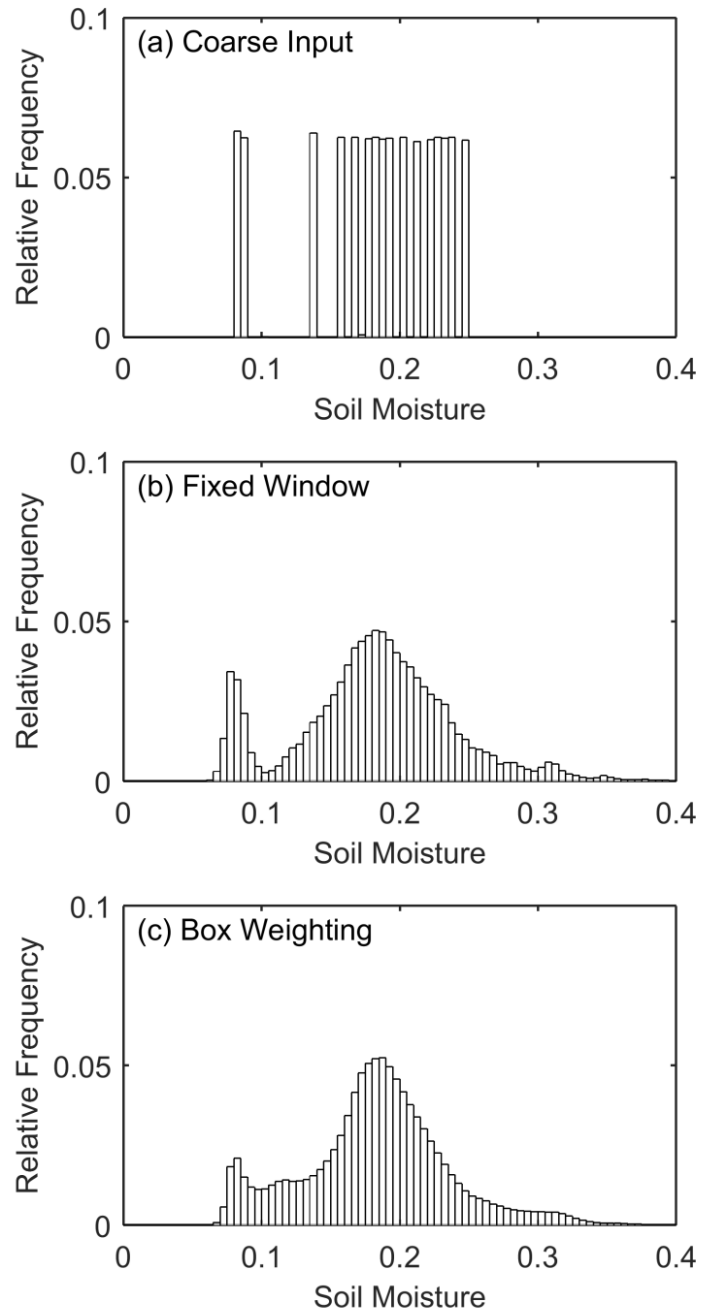


Figure 11. Histograms of soil moisture for Eastern Victoria on 01 Nov 08 using (a) the coarse resolution input, (b) the fine resolution output from the fixed window procedure, and (c) the fine resolution output from the shifting window procedure with box weighting.

7. REFERENCES

- AFWA (2002), Data Format Handbook for AGRMET.
- Bartalis, Z., W. Wagner, V. Naeimi, S. Hasenauer, K. Scipal, H. Bonekamp, J. Figa and C. Anderson (2007), Initial soil moisture retrievals from the METOP-A Advanced Scatterometer (ASCAT), *Geophysical Research Letters*, 34(20), 1-5. doi: 10.1029/2007gl091088.
- Bartsch, A., H. Balzter and C. George (2009), The influence of regional surface soil moisture anomalies on forest fires in Siberia observed from satellites, *Environmental Research Letters*, 4(4), 1-9. doi: 10.1088/1748-9326/4/4/045021.
- Beck, H. E., R. A. M. de Jeu, J. Schellekens, A. I. J. M. van Dijk and L. A. Bruijnzeel (2009), Improving Curve Number Based Storm Runoff Estimates Using Soil Moisture Proxies, *Ieee Journal of Selected Topics in Applied Earth Observations and Remote Sensing*, 2(4), 250-259. doi: 10.1109/Jstars.2009.2031227.
- Bolten, J. D., W. T. Crow, X. W. Zhan, T. J. Jackson and C. A. Reynolds (2010), Evaluating the Utility of Remotely Sensed Soil Moisture Retrievals for Operational Agricultural Drought Monitoring, *Ieee Journal of Selected Topics in Applied Earth Observations and Remote Sensing*, 3(1), 57-66. doi: 10.1109/Jstars.2009.2037163.
- Busch, F. A., J. D. Niemann and M. Coleman (2012), Evaluation of an empirical orthogonal function-based method to downscale soil moisture patterns based on topographical attributes, *Hydrological Processes*, 26(18), 2696-2709. doi: 10.1002/hyp.8363.
- Chapin, E., A. Chau, J. Chen, B. Heavey, S. Hensley, Y. L. Lou, R. Machuzak and M. Moghaddam (2012), AirMOSS: An Airborne P-band SAR to Measure Root-Zone Soil Moisture, 2012 IEEE Radar Conference (Radar), 693-698.
- Chauhan, N. S., S. Miller and P. Ardanuy (2003), Spaceborne soil moisture estimation at high resolution: a microwave-optical/IR synergistic approach, *International Journal of Remote Sensing*, 24(22), 4599-4622. doi: 10.1080/0143116031000156837.
- Coleman, M. L. and J. D. Niemann (2012), An evaluation of nonlinear methods for estimating catchment-scale soil moisture patterns based on topographic attributes, *Journal of Hydroinformatics*, 14(3), 800-814. doi: 10.2166/hydro.2012.145.
- Coleman, M. L. and J. D. Niemann (2013), Controls on topographic dependence and temporal instability in catchment-scale soil moisture patterns, *Water Resources Research*, 49(3), 1625-1642. doi: 10.1002/wrcr.20159.
- Crow, W. T., E. F. Wood and R. Dubayah (2000), Potential for downscaling soil moisture maps derived from spaceborne imaging radar data, *Journal of Geophysical Research-Atmospheres*, 105(D2), 2203-2212. doi: 10.1029/1999jd901010.

- Das, N. N., D. Entekhabi and E. G. Njoku (2011), An Algorithm for Merging SMAP Radiometer and Radar Data for High-Resolution Soil-Moisture Retrieval, *IEEE Transactions on Geoscience and Remote Sensing*, 49(5), 1504-1512. doi: 10.1109/Tgrs.2010.2089526.
- de Wit, A. M. and C. A. van Diepen (2007), Crop model data assimilation with the Ensemble Kalman filter for improving regional crop yield forecasts, *Agricultural and Forest Meteorology*, 146(1-2), 38-56. doi: 10.1016/j.agrformet.2007.05.004.
- Delworth, T. and S. Manabe (1989), The Influence of Soil Wetness on near-Surface Atmospheric Variability, *Journal of Climate*, 2(12), 1447-1462. doi: 10.1175/1520-0442(1989)002<1447:Tioswo>2.0.Co;2.
- Dingman, S. L. (2002), *Physical Hydrology*, 2nd ed., 646 pp, Prentice Hall, Upper Saddle River, N. J.
- Dirmeyer, P. A. (1999), Assessing GCM sensitivity to soil wetness using GSWP data, *Journal of the Meteorological Society of Japan*, 77(1B), 367-385.
- Dunne, T. and R. D. Black (1970), Partial Area Contributions to Storm Runoff in a Small New-England Watershed, *Water Resources Research*, 6(5), 1296-1311. doi: 10.1029/Wr006i005p01296.
- Entekhabi, D., E. G. Njoku, P. E. O'Neill, K. H. Kellogg, W. T. Crow, W. N. Edelstein, J. K. Entin, S. D. Goodman, T. J. Jackson, J. Johnson, J. Kimball, J. R. Piepmeier, R. D. Koster, N. Martin, K. C. McDonald, M. Moghaddam, S. Moran, R. Reichle, J. C. Shi, M. W. Spencer, S. W. Thurman, L. Tsang and J. Van Zyl (2010), The Soil Moisture Active Passive (SMAP) Mission, *IEEE*, 98(5), 704-716. doi: 10.1109/Jproc.2010.2043918.
- Entekhabi, D., I. Rodriguez-Iturbe and F. Castelli (1996), Mutual interaction of soil moisture state and atmospheric processes, *Journal of Hydrology*, 184(1-2), 3-17. doi: 10.1016/0022-1694(95)02965-6.
- Famiglietti, J. S., J. W. Rudnicki and M. Rodell (1998), Variability in surface moisture content along a hillslope transect: Rattlesnake Hill, Texas, *Journal of Hydrology*, 210(1-4), 259-281. doi: 10.1016/S0022-1694(98)00187-5.
- Fang, B. and V. Lakshmi (2014), Soil moisture at watershed scale: Remote sensing techniques, *Journal of Hydrology*, 516, 258-272. doi: 10.1016/j.jhydrol.2013.12.008.
- Ferranti, L. and P. Viterbo (2006), The European summer of 2003: Sensitivity to soil water initial conditions, *Journal of Climate*, 19(15), 3659-3680. doi: 10.1175/Jcli3810.1.
- Flores, A. N., D. Entekhabi and R. L. Bras (2014), Application of a hillslope-scale soil moisture data assimilation system to military trafficability assessment, *Journal of Terramechanics*, 51, 53-66. doi: 10.1016/j.jterra.2013.11.004.

- Gomez-Plaza, A., M. Martinez-Mena, J. Albaladejo and V. M. Castillo (2001), Factors regulating spatial distribution of soil water content in small semiarid catchments, *Journal of Hydrology*, 253(1-4), 211-226. doi: 10.1016/S0022-1694(01)00483-8.
- Hirano, A., R. Welch and H. Lang (2003), Mapping from ASTER stereo image data: DEM validation and accuracy assessment, *ISPRS Journal of Photogrammetry and Remote Sensing*, 57(5-6), 356-370. doi: 10.1016/S0924-2716(02)00164-8.
- Horn, R. and H. Fleige (2003), A method for assessing the impact of load on mechanical stability and on physical properties of soils, *Soil & Tillage Research*, 73(1-2), 89-99. doi: 10.1016/S0167-1987(03)00102-8.
- Houser, P. R., W. J. Shuttleworth, J. S. Famiglietti, H. V. Gupta, K. H. Syed and D. C. Goodrich (1998), Integration of soil moisture remote sensing and hydrologic modeling using data assimilation, *Water Resources Research*, 34(12), 3405-3420. doi: 10.1029/1998wr900001.
- Jones, A. S. and T. H. Vonder Haar (2002), A dynamic parallel data-computing environment for cross-sensor satellite data merger and scientific analysis, *Journal of Atmospheric and Oceanic Technology*, 19(9), 1307-1317. doi: 10.1175/1520-0426(2002)019<1307:Adpdce>2.0.Co;2.
- Kaheil, Y. H., M. K. Gill, M. Mckee, L. A. Bastidas and E. Rosero (2008), Downscaling and assimilation of surface soil moisture using ground truth measurements, *IEEE Transactions on Geoscience and Remote Sensing*, 46(5), 1375-1384. doi: 10.1109/Tgrs.2008.916086.
- Kasischke, E. S., L. L. Bourgeau-Chavez and J. F. Johnstone (2007), Assessing spatial and temporal variations in surface soil moisture in fire-disturbed black spruce forests in Interior Alaska using spaceborne synthetic aperture radar imagery - Implications for post-fire tree recruitment, *Remote Sensing of Environment*, 108(1), 42-58. doi: 10.1016/j.rse.2006.10.020.
- Kerr, Y. H., P. Waldteufel, P. Richaume, J. P. Wigneron, P. Ferrazzoli, A. Mahmoodi, A. Al Bitar, F. Cabot, C. Gruhier, S. E. Juglea, D. Leroux, A. Mialon and S. Delwart (2012), The SMOS Soil Moisture Retrieval Algorithm, *IEEE Transactions on Geoscience and Remote Sensing*, 50(5), 1384-1403. doi: 10.1109/Tgrs.2012.2184548.
- Kerr, Y. H., P. Waldteufel, J. P. Wigneron, S. Delwart, F. Cabot, J. Boutin, M. J. Escorihuela, J. Font, N. Reul, C. Gruhier, S. E. Juglea, M. R. Drinkwater, A. Hahne, M. Martin-Neira and S. Mecklenburg (2010), The SMOS Mission: New Tool for Monitoring Key Elements of the Global Water Cycle, *Proceedings of the IEEE*, 98(5), 666-687. doi: 10.1109/Jproc.2010.2043032.

- Kim, G. and A. P. Barros (2002), Downscaling of remotely sensed soil moisture with a modified fractal interpolation method using contraction mapping and ancillary data, *Remote Sensing of Environment*, 83(3), 400-413. doi: 10.1016/S0034-4257(02)00044-5.
- Koster, R. D. and M. J. Suarez (2003), Impact of land surface initialization on seasonal precipitation and temperature prediction, *Journal of Hydrometeorology*, 4(2), 408-423. doi: 10.1175/1525-7541(2003)4<408:Iolsio>2.0.Co;2.
- Lakshmi, V. (1998), Special sensor microwave imager data in field experiments: FIFE-1987, *International Journal of Remote Sensing*, 19(3), 481-505. doi: 10.1080/014311698216116.
- Li, L., P. W. Gaiser, B. C. Gao, R. M. Bevilacqua, T. J. Jackson, E. G. Njoku, C. Rudiger, J. C. Calvet and R. Bindlish (2010), WindSat Global Soil Moisture Retrieval and Validation, *IEEE Transactions on Geoscience and Remote Sensing*, 48(5), 2224-2241. doi: 10.1109/Tgrs.2009.2037749.
- Mahfouf, J. F., E. Richard and P. Mascart (1987), The Influence of Soil and Vegetation on the Development of Mesoscale Circulations, *Journal of Climate and Applied Meteorology*, 26(11), 1483-1495. doi: 10.1175/1520-0450(1987)026<1483:Tiosav>2.0.Co;2.
- Mascaro, G., E. R. Vivoni and R. Deidda (2011), Soil moisture downscaling across climate regions and its emergent properties, *Journal of Geophysical Research-Atmospheres*, 116. doi: 10.1029/2011jd016231.
- Merlin, O., A. Chehbouni, Y. H. Kerr and D. C. Goodrich (2006), A downscaling method for distributing surface soil moisture within a microwave pixel: Application to the Monsoon '90 data, *Remote Sensing of Environment*, 101(3), 379-389. doi: 10.1016/j.rse.2006.01.004.
- Merlin, O., A. G. Chehbouni, Y. H. Kerr, E. G. Njoku and D. Entekhabi (2005), A combined modeling and multipectral/multiresolution remote sensing approach for disaggregation of surface soil moisture: Application to SMOS configuration, *IEEE Transactions on Geoscience and Remote Sensing*, 43(9), 2036-2050. doi: 10.1109/Tgrs.2005.853192.
- Merlin, O., M. J. Escorihuela, M. A. Mayoral, O. Hagolle, A. Al Bitar and Y. Kerr (2013), Self-calibrated evaporation-based disaggregation of SMOS soil moisture: An evaluation study at 3 km and 100 m resolution in Catalunya, Spain, *Remote Sensing of Environment*, 130, 25-38. doi: 10.1016/j.rse.2012.11.008.
- Merlin, O., C. Rudiger, A. Al Bitar, P. Richaume, J. P. Walker and Y. H. Kerr (2012), Disaggregation of SMOS Soil Moisture in Southeastern Australia, *IEEE Transactions on Geoscience and Remote Sensing*, 50(5), 1556-1571. doi: 10.1109/Tgrs.2011.2175000.
- Montosi, E., S. Manzoni, A. Porporato and A. Montanari (2012), An eco-hydrologic model of malaria outbreaks, *Hydrology and Earth System Sciences*, 9, 2831-2854.

- Nash, J. E. and J. V. Sutcliffe (1970), River flow forecasting through conceptual models part I - a discussion of principles, *Journal of Hydrology*, 10, 282-290.
- Njoku, E. G., T. J. Jackson, V. Lakshmi, T. K. Chan and S. V. Nghiem (2003), Soil moisture retrieval from AMSR-E, *IEEE Transactions on Geoscience and Remote Sensing*, 41(2), 215-229. doi: 10.1109/Tgrs.2002.808243.
- Pellenq, J., J. Kalma, G. Boulet, G. M. Saulnier, S. Wooldridge, Y. Kerr and A. Chehbouni (2003), A disaggregation scheme for soil moisture based on topography and soil depth, *Journal of Hydrology*, 276(1-4), 112-127. doi: 10.1016/S0022-1694(03)00066-0.
- Perry, M. A. and J. D. Niemann (2007), Analysis and estimation of soil moisture at the catchment scale using EOFs, *Journal of Hydrology*, 334(3-4), 388-404. doi: 10.1016/j.jhydrol.2006.10.014.
- Ranney, K. J., J. D. Niemann, B. M. Lehman, T. R. Green and A. S. Jones (2015), A method to downscale soil moisture to fine resolutions using topographic, vegetation, and soil data, *Advances in Water Resources*, 76, 81-96. doi: 10.1016/j.advwatres.2014.12.003.
- Sahoo, A. K., G. J. M. De Lannoy, R. H. Reichle and P. R. Houser (2013), Assimilation and downscaling of satellite observed soil moisture over the Little River Experimental Watershed in Georgia, USA, *Advances in Water Resources*, 52, 19-33. doi: 10.1016/j.advwatres.2012.08.007.
- Seuffert, G., P. Gross, C. Simmer and E. F. Wood (2002), The influence of hydrologic modeling on the predicted local weather: Two-way coupling of a mesoscale weather prediction model and a land surface hydrologic model, *Journal of Hydrometeorology*, 3(5), 505-523. doi: 10.1175/1525-7541(2002)003<0505:Tiohmo>2.0.Co;2.
- Shoop, S., R. Affleck, C. Collins, G. Larsen, L. Barna and P. Sullivan (2005), Maneuver analysis methodology to predict vehicle impacts on training lands, *Journal of Terramechanics*, 42(3-4), 281-303. doi: 10.1016/j.jterra.2004.10.012.
- Song, C. Y., L. Jia and M. Menenti (2014), Retrieving High-Resolution Surface Soil Moisture by Downscaling AMSR-E Brightness Temperature Using MODIS LST and NDVI Data, *IEEE Journal of Selected Topics in Applied Earth Observations and Remote Sensing*, 7(3), 935-942. doi: 10.1109/Jstars.2013.2272053.
- Tabatabaenejad, A., M. Burgin, X. Y. Duan and M. Moghaddam (2015), P-Band Radar Retrieval of Subsurface Soil Moisture Profile as a Second-Order Polynomial: First AirMOSS Results, *IEEE Transactions on Geoscience and Remote Sensing*, 53(2), 645-658. doi: 10.1109/Tgrs.2014.2326839.

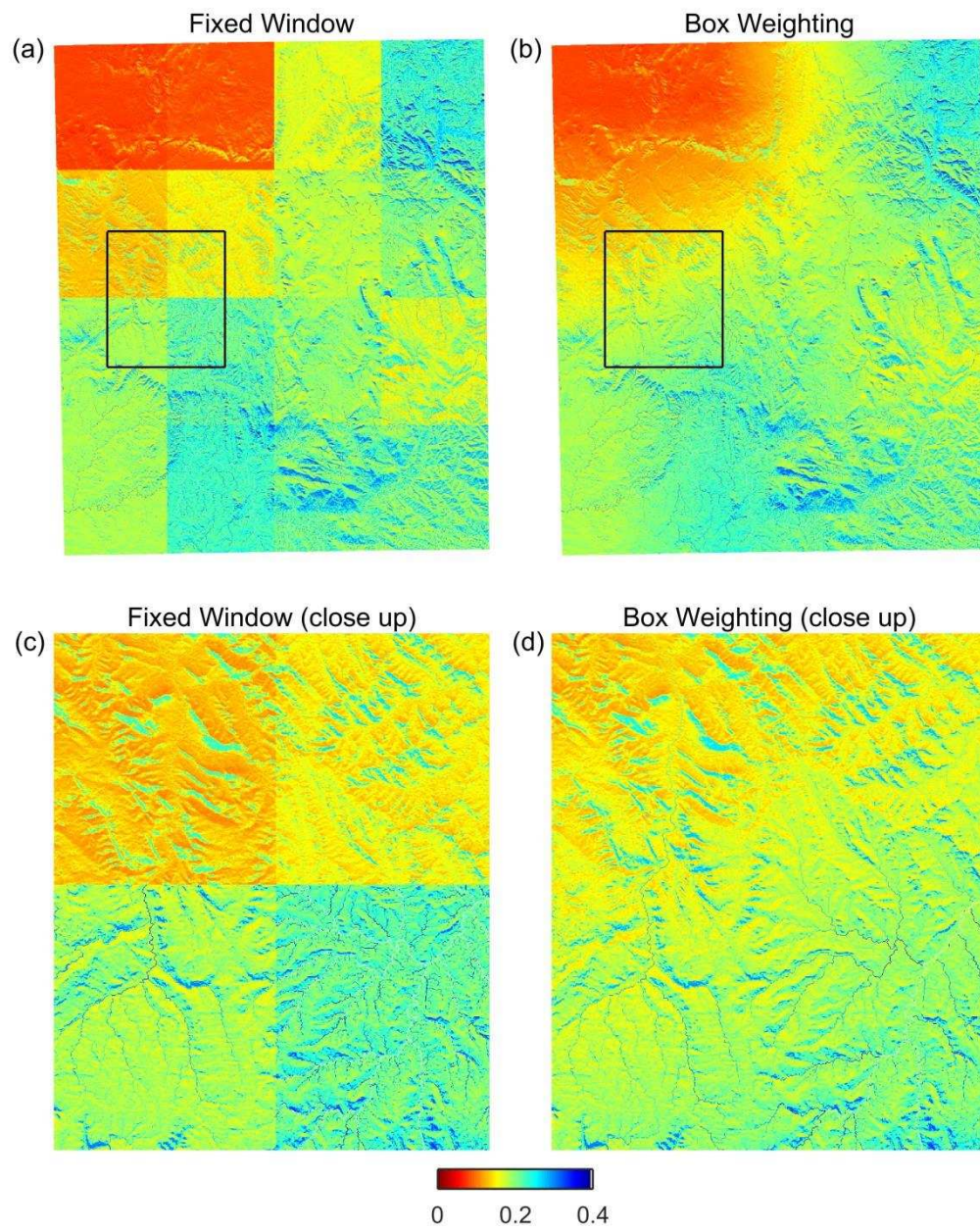
- Temimi, M., R. Leconte, N. Chaouch, P. Sukumal, R. Khanbilvardi and F. Brissette (2010), A combination of remote sensing data and topographic attributes for the spatial and temporal monitoring of soil wetness, *Journal of Hydrology*, 388(1-2), 28-40. doi: 10.1016/j.jhydrol.2010.04.021.
- Vero, S. E., D. L. Antille, S. T. J. Lalor and N. M. Holden (2014), Field evaluation of soil moisture deficit thresholds for limits to trafficability with slurry spreading equipment on grassland, *Soil Use and Management*, 30(1), 69-77. doi: 10.1111/sum.12093.
- Walker, J. P., G. R. Willgoose and J. D. Kalma (2001), The Nerrigundah data set: Soil moisture patterns, soil characteristics, and hydrological flux measurements, *Water Resources Research*, 37(11), 2653-2658. doi: 10.1029/2001wr000545.
- Werbylo, K. L. and J. D. Niemann (2014), Evaluation of sampling techniques to characterize topographically-dependent variability for soil moisture downscaling, *Journal of Hydrology*, 516, 304-316. doi: 10.1016/j.jhydrol.2014.01.030.
- Western, A. W. and R. B. Grayson (1998), The Tarrawarra data set: Soil moisture patterns, soil characteristics, and hydrological flux measurements, *Water Resources Research*, 34(10), 2765-2768. doi: 10.1029/98wr01833.
- Western, A. W., R. B. Grayson, G. Bloschl, G. R. Willgoose and T. A. McMahon (1999), Observed spatial organization of soil moisture and its relation to terrain indices, *Water Resources Research*, 35(3), 797-810. doi: 10.1029/1998wr900065.
- Wilson, D. J., A. W. Western and R. B. Grayson (2005), A terrain and data-based method for generating the spatial distribution of soil moisture, *Advances in Water Resources*, 28(1), 43-54. doi: 10.1016/j.advwatres.2004.09.007.
- Wood, E. F. (1997), Effects of soil moisture aggregation on surface evaporative fluxes, *Journal of Hydrology*, 190, 397-412.
- Yamaguchi, Y., A. B. Kahle, H. Tsu, T. Kawakami and M. Piel (1998), Overview of Advanced Spaceborne Thermal Emission and Reflection Radiometer (ASTER), *IEEE Transactions on Geoscience and Remote Sensing*, 36(4), 1062-1071. doi: 10.1109/36.700991.

8. APPENDICIES

8.1 APPENDIX A

	Parameter	Tarrawarra			Nerrigundah			Cache la Poudre		
		Lower	Upper	Calibrated	Lower	Upper	Calibrated	Lower	Upper	Calibrated
Climate	E_p (mm/day)	2.25	2.25	2.25	2.81	2.81	2.81	2.55	2.55	2.55
	α	0.26	0.26	0.26	0.26	0.26	0.26	0.26	0.26	0.26
Vegetation	β_r	0.2	5	3.55	0.2	5	1.60	0.2	5	5.00
	β_a	0.2	5	5	0.2	5	5	0.2	5	3.6002
	λ	0	1	0.37	0	1	0.96	0	1	0.89
	η	0.01	1	0.83	0.01	1	1.00	0.01	1	0.04
	μ	1	1	1	1	1	1	1	3	1.92
	ζ (m)	1	1	1.000	1	1	1.000	0.001	200	0.026
	V	1.0	1.0	1.0	1.0	1.0	1.0	1.0	1.0	1.0
Soil	ϕ (m ³ /m ³)	0.29	0.70	0.700	0.41	0.56	0.435	0.38	0.41	0.409
	$K_{s,v}$ (mm/day)	17	3355	386.3	36	2592	36.0	936	1845	984.9
	t	1	500	47.2	1	500	209.4	1	500	75.4
	γ_h	1	36.2	6.92	1	29.92	5.01	1	19.3	14.36
	γ_v	6.68	36.2	14.12	6.3	29.92	29.15	6.3	19.3	14.10
	δ_0 (m)	0.3	0.3	0.3	0.25	0.25	0.25	0.05	0.05	0.05
	κ_{min} (1/m)	-1000000	-0.009	-886375	-1000000	-0.0057	-643233	-1000000	-0.056	-651810
	ε	1	3	1	1	3	1	1	3	3

8.2 APPENDIX B



8.3 APPENDIX C

